the detector output are presented. The chevron linewidth in particular is shown to be a design parameter that has a strong influence on the signal. Optimized detectors using 2.1-μm chevron linewidth patterned in 0.44-μm thick Permalloy at 0.82-μm spacing on 3.37-μm epi films have a dV/V figure of merit of 0.5% for 35-40 Oe drive fields.

ACKNOWLEDGMENTS

It is a pleasure to thank A. H. Bobeck, P. I. Bonyhard, and J. E. Geusic for helpful suggestions in this work, and D. A. Ferrier and W. C. Richold for expert technical assistance.

REFERENCES

[1] G. S. Almasi, "Bubble Domain Propagation and Sensing," *Proc. IEEE*, 61, 438-444 (1973). George S. Almasi, "Magnetic Bubble-Domain Detection: Review and Outlook," *IEEE Trans. Magnetics*, MAG-9, 663-669 (1973).

[2] A. H. Bobeck, I. Danylchuk, F. C. Rossol, and W. Strauss, "Evolution of Bubble Circuits Processed by a Single Mask Level," *IEEE Trans. Magnetics*, MAG-9, 474-480 (1973).

[3] A. H. Bobeck, P. I. Bonyhard, and J. E. Geusic, "Magnetic Bubbles–An Emerging New Memory Technology," *Proc. IEEE*, 63, 1176 (1975).

[4] P. K. George, T. R. Oeffinger and T. T. Chen, "Magnetoresistance and Noise Properties of Chevron Stretcher Detectors for Field Access Bubble Domain Devices," *J. Appl. Phys.*, 47, 3302 (1976).

[5] K. Komenou, H. Nakajima, and K. Asama, "Permalloy Film for Single-Level Detector With High Sensitivity," *AIP Conf. Proc.*, 24, 554-555 (1975).

[6] A. A. Thiele, "Theory of Static Stability of Cylindrical Domains in Uniaxial Platelets," *J. Appl. Physics*, 41, 1139 (1970).

[7] G. P. Vella-Coleiro and T. J. Nelson, "Stroboscopic Observation of Magnetic Bubble Circuits Using a Gated Image-Intensifier Tube," *Appl. Phys. Letters*, 24, 397-398 (1974).

Induction Heating for Case Hardening Applications

FREDERICK J. YOUNG, SENIOR MEMBER, IEEE

Abstract—**It is observed that the equations describing induction heating in ferromagnetic materials are rather nonlinear. Although the thermal properties are nonlinear, the greatest nonlinearity arises from the ferromagnetic behavior of the material. A way of circumventing this difficulty while retaining the important magnetization curve is presented. A numerical solution accounting for temperature variations in the saturation magnetization, electrical and thermal conductivities, and specific heat is presented. It is found for case hardening applications that only a narrow near surface region heats to the vicinity of the Curie temperature, and a simple theory describing this region is derived. Just beyond the near surface region a sharp temperature gradient results which is of importance in case hardening. A simple expression for the gradient is developed. These expressions, verified by a complete numerical analysis, aid in the choice of an induction heating excitation system for case hardening applications.**

INTRODUCTION

INDUCTION heating is used for melting, forging, hardening, brazing, welding and many other applications amounting to a multimillion dollar business each year. Powers ranging from a new hundred watts to almost 100 megawatts at frequencies ranging from 50 hertz to several megahertz are utilized. Many of these processes are described by Tudbury [1], [2].

Induction heating problems involving paramagnetic materials, e.g., copper, silver, brass, etc., can be solved by the straightforward application of Maxwell's electrodynamic equations and the heat flow equations. The solutions are complex but can be handled by digital computation. The same approach to induction heating in ferromagnetic materials leads to difficulties not amenable to digital computation. These are the same difficulties encountered in the analyses of shielding by ferromagnetic materials [3]. Computational difficulties are encountered because of the marked variation in permeability as a function of magnetic field intensity. Fortunately these difficulties are circumvented by the use of the limiting nonlinear methods set forth in earlier works [4], [5]. The solutions to the limiting nonlinear theory are actually simpler than those obtained for paramagnetic substances by the aforementioned straightforward solution of Maxwell's equations.

It is the goal of this paper to establish a method for the prediction of the transient temperature distribution in a ferromagnetic material being heated by electromagnetic induction. The prediction, obtained by the application of the limiting nonlinear theory and the equation of heat transfer, is based on

Manuscript received November 5, 1975; revised March 25, 1977.

The author is with the Department of Electrical Engineering, Pennsylvania State University, University Park, PA 16802.

the applied magnetic field intensity, its frequency, the physical properties of the ferromagnetic material (electrical and thermal conductivity, heat capacity, density, saturation induction), geometry, and surface cooling. This information is to be used to determine the values of the applied magnetic intensity and frequency necessary for controlled induction heating.

The Basic Equations of Induction Heating

Because alternating electromagnetic fields are used to produce heat in the work pieces, the solution to the induction heating problem is derived from the simultaneous solution of Maxwell's equations and the equations of heat transfer. Because of the wide range of temperatures present, the physical properties of the material do not remain constant and must be considered as functions of local temperature. The Maxwell equations are

$$\nabla \times E = -\partial B/\partial t \tag{1}$$

$$\nabla \times H = \sigma E \tag{2}$$

where E is electric field intensity, B is the magnetic induction, H is the magnetic field intensity, and σ is electrical conductivity. The equation of heat transfer is given by

$$\nabla \cdot \kappa \nabla T + p = \rho c \frac{\partial T}{\partial t}, \tag{3}$$

a result of the law of conservation of energy and Fourier's law of heat conduction. Here T is the temperature, ρ is the density, c is the heat capacity, κ is the thermal conductivity, and p is the instantaneous volumetric power density. The density is sensibly constant, but c and κ vary strongly with temperature. The power density is given by $(\nabla \times H)^2/\sigma$, and is a strong function of temperature also. Equations (1) and (2) can be combined to eliminate the electric field intensity. There results

$$\nabla \times \frac{1}{\sigma} \nabla \times H = -\frac{\partial B}{\partial t} = -\mu_{\text{inc}} \frac{\partial H}{\partial t} \tag{4}$$

which is highly nonlinear. Here $\mu_{\text{inc}} = \partial B/\partial H$, the incremental permeability. To solve the induction heating in general, (3) and (4) must be solved simultaneously in three dimensions in work piece, exciting coil, and in all the rest of space. In this paper only one-dimensional spatial variations are considered, namely the case of semi-infinite slabs or sheets. In that case (3) and (4) become

$$\frac{\partial}{\partial y}\left(\kappa \frac{\partial T}{\partial y}\right) + \frac{1}{\sigma}\left(\frac{\partial H}{\partial y}\right)^2 = \rho c \frac{\partial T}{\partial t} \tag{5}$$

and

$$\frac{\partial}{\partial y}\left(\frac{1}{\sigma}\frac{\partial H}{\partial y}\right) = \mu_{\text{inc}} \frac{\partial H}{\partial t}. \tag{6}$$

Even without considering the variation of σ and μ_{inc} with temperature, (6) is highly nonlinear because μ_{inc} varies so strongly with H. In this paper the limiting nonlinear analysis of McConnell [4] and Agarwal [5] is modified to include thermal effects and combined with (5). For the purpose of comparison (5) first is assumed to have constant values to κ, σ, ρ, and c so that an analytical solution can be obtained. Later σ, κ, c, and B_s (the saturation induction) are allowed to vary with temperature, and a numerical solution is obtained. The purely linear thermal solution, the first to recognize the inherent nonlinearity of the ferromagnetic material, only provides some insight to the nature of the more accurate numerical solution.

Basic Electromagnetic Phenomena in Ferromagnetic Media

Consider the induction heating of a thick ferromagnetic slab by the application of a tangential magnetic field of intensity $H_M \sin \omega t$. In the steady state (which exists after a few cycles), regions of saturation form at the surface early in each half cycle of magnetization and travel inward (in the y direction) till they reach the depth of penetration δ. A typical positive half-cycle configuration is shown in Fig. 1. Whilst sin ωt is positive, the positively saturated region of width ζ propagates in the y direction, annihilating the region of negative saturation left by the previous half-cycle. When sin ωt reverses, a region of reverse saturation forms at the surface and travels toward $y = \delta$, annihilating the region of positive saturation in the process. McConnell [4] and Agarwal [5] show that a spatially constant current density in the x direction is induced in the growing region of saturation. The induced current causes the ferromagnetic material to heat. The depth of penetration δ is given by [3], [4], [5]

$$\delta = \sqrt{H_M/\pi \sigma f B_s} \tag{7}$$

where f is frequency, H_M is the maximum value of the applied magnetic field intensity, B_s is the saturation induction, and σ is the electrical conductivity. The distribution of current density, magnetic field intensity, and magnetic induction in the limiting nonlinear approximate theory of magnetization is given in Fig. 2. As the positive half-cycle of excitation progresses, the regions of positive saturation and constant negative current move from the origin toward their ultimate limit δ, the depth of penetration. When the applied magnetic intensity becomes negative, saturation forms at $y = 0$ and progresses from the origin to $y = \delta$. In this analysis, it is assumed the work piece is much thicker than the ferromagnetic skin depth δ so that the regions of saturation originating from each material face never meet at center. The location of the boundary between the regions of positive and negative saturation is given by Agarwal as

$$\zeta = \delta \sin\left(\frac{\omega t}{2}\right) \tag{8}$$

which is valid for $0 \leqslant t \leqslant \pi/\omega$ or during any positive half-cycle of excitation. A similar expression can be written for the negative half-cycle of excitation, during which ζ behaves the same as during the positive half-cycle. The electric field in the x direction is given by

$$E_x = -\frac{2H_M}{\sigma\delta} \cos \omega t/2, \qquad 0 < y \leqslant \zeta$$

$$= 0, \qquad y > \zeta \tag{9}$$

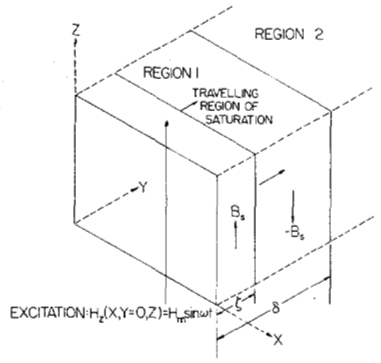

Fig. 1. Geometry considered.

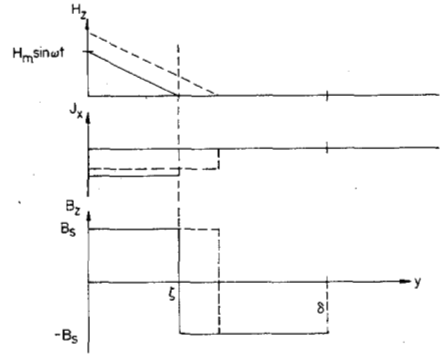

Fig. 2. Field distribution in skin region of limiting nonlinear model of the ferromagnetic material (——— at some time during the positive half-cycle of excitation, – – – at a slightly later time).

during the positive half-cycle of excitation. During the negative half-cycle of excitation, the sign of the electric field reverses but the waveform remains identical to that existing in the positive half-cycle. The magnetic field in the x direction is given by

$$H_z = (1 - y/\delta) H_M \sin \omega t, \quad (0 < y \leqslant \zeta)$$
$$= 0, \quad y > \zeta \tag{10}$$

during the positive half-cycles of excitation. During negative half-cycle of excitation the space distribution and waveform remain the same, but the sign of H_z reverses. A good portrayal of these fields is given in Figs. 6 and 7 of Agarwal [5]. According to Agarwal [5] the average power per unit volume generated by the uniformly distributed time varying current density in the skin region is

$$\langle P \rangle = \frac{8}{3\pi} \frac{H_M^2}{\sigma \delta^2}, \tag{11}$$

or by making use of (7)

$$\langle P \rangle = \frac{8}{3} H_M B_s f. \tag{12}$$

From (12) it is clear that the average power density is a function of the applied field, frequency, and saturation induction.

If the temperature of any portion of the work piece approaches or exceeds the Curie temperature, the material in that region becomes paramagnetic and the solutions become easy to obtain when spatial temperature variation is not included. The solutions found in most electrodynamics texts are

$$H_z = H_M \exp(-y/\delta_c) \sin(\omega t - y/\delta_c) \tag{13}$$

$$E_x = \frac{\sqrt{2} H_M}{\sigma \delta_c} \exp(-y/\delta_c) \cos(\omega t - y/\delta_c) \tag{14}$$

where δ_c is the depth of penetration at which the fields are attenuated to $1/\epsilon$ of their surface values. Here $\delta_c = \sqrt{1/\pi f \sigma \mu}$, which has the same form as (7). These expressions are identical if one lets $\mu = B_s/H_M$. By comparing (9) and (10) to (14) and (13), it is clear that the limiting nonlinear and the conventional theory yield similar results. However, the limiting nonlinear theory is the simplest because all the variation of field quantities occurs within the depth of penetration δ. Beyond the depth of penetration E and H are zero. The conventional theory of (13) and (14) yields a power dissipation per unit volume of

$$P_c = H_M^2 / 2\sigma\delta_c^2. \tag{15}$$

Here the total power dissipated in the region $0 < y < \infty$ is found and divided by δ_c to obtain (15) [5]. This yields an estimate of the power density in the skin region which is about 15.7% high. The remaining power is dissipated beyond the skin region in contrast to the limiting nonlinear case where no heating occurs beyond the depth of penetration.

An Approximate Solution

It is assumed that the period of the electrical excitation is much smaller than the thermal time constant of the ferromagnetic material. Then the effective or average power is assumed to be applied in the whole skin region. Because the total thickness of the ferromagnetic material is much greater than the skin depth δ, it is assumed that the temperature is only a function of time in the skin region and that the heat capacity and thermal conductivity are constant (see Table I). This is consistent with the relatively high thermal conductivity of ferromagnetic materials. The skin region is denoted as region 1 on Fig. 1. In the skin region the temperature is not a function of y under this assumption. In region 2 the temperature varies with both position and time. The temperature in region 2 obeys the diffusion equation

$$\kappa \frac{\partial^2 T_2}{\partial y^2} = \rho c \frac{\partial T_2}{\partial t} \tag{16}$$

where T_2 is the temperature in region 2, κ is the thermal conductivity, ρ is the density, and c the specific heat of the ferromagnetic material. Region 1 obeys the same diffusion equation with the power generation term added. It is given by

$$\kappa \frac{\partial^2 T_1}{\partial y^2} + P = \rho c \frac{\partial T_1}{\partial t} \tag{17}$$

which is averaged over the thickness of region 1. There results

$$\frac{\kappa}{\delta} \frac{\partial T_1}{\partial y}\bigg|_{y=\delta} - \frac{\kappa}{\delta} \frac{\partial T_1}{\partial y}\bigg|_{y=0} + \langle P \rangle = \rho c \frac{d\langle T_1 \rangle}{dt}. \tag{18}$$

TABLE I
PHYSICAL PROPERTIES OF SOME FERROMAGNETIC MATERIALS AT ROOM TEMPERATURE

Material	Saturation Induction B_s (Kilogauss)	Coercive Force H_c (oersted)	Curie Temperature °C	Density g/cm^3	Electrical Conductivity MHO/METER	Thermal Conductivity cal/sq cm/cm/°K/sec	Specific Heat cal/g/°K
Cobalt	18.7	8.9	1115	8.9	1.6×10^7	0.165	0.099
Iron	21.7	0.14-0.54	770	7.88	1.03×10^7	0.18	0.11
Nickel	6.1	0.42	680	8.89	1.46×10^7	0.22	0.105

From Newton's Law of Cooling,

$$\kappa \left.\frac{\partial T_1}{\partial y}\right|_{y=0} = hT_1\,(y=0)$$

where h is the cooling or film coefficient and T_1 and T_2 are the temperature rises above ambient. By the use of Newton's Law of Cooling (18) becomes

$$\rho c\delta \frac{d\langle T_1\rangle}{dt} + h\langle T_1\rangle = \langle P\rangle \delta + \kappa \left.\frac{\partial T_1}{\partial y}\right|_{y=\delta} \tag{19}$$

where it is assumed $T_1(y=0) = \langle T_1\rangle$ is the average temperature in region 1. Equation (19) can be verified by applying the law of conservation of energy to the small part of region 1 being situated between y and $y+\Delta y$. It is interesting to observe that the power entering an $x-z$ surface area heats the entire ferromagnetic material. That power is given by

$$p = \langle P\rangle\delta = \frac{4}{3} H_M^{3/2} \sqrt{\frac{\pi f B_s}{\sigma}} \tag{20}$$

which is a strong function of applied field and a weaker function of frequency and material properties. Equations (16) and (19) are solved simultaneously subject to the conditions that before H_M is applied, $\langle T_1\rangle = T_2 = 0$ for all

$$y>0,\ T_2(y=\infty, t) = 0,\ \langle T\rangle_1|_{y=\delta} = T_2|_{y=\delta}$$

and

$$\left.\frac{\partial T_1}{\partial y}\right|_{y=\delta} = \left.\frac{\partial T_2}{\partial y}\right|_{y=\delta}.$$

The average temperature in region 1 derived in the appendix is given by

$$\langle T_1\rangle = \frac{\langle P\rangle}{\rho c(a-b)}\left[\frac{(1-e^{b^2 t}\operatorname{erfc} b\sqrt{t})}{b} - \frac{(1-e^{a^2 t}\operatorname{erfc} a\sqrt{t})}{a}\right] \tag{21}$$

where

$$a = \frac{1}{2\delta}\sqrt{\frac{\kappa}{\rho c}}\left[1+\sqrt{1-\frac{4h\delta}{\kappa}}\right]$$

and

$$b = \frac{1}{2\delta}\sqrt{\frac{\kappa}{\rho c}}\left[1-\sqrt{1-\frac{4h\delta}{\kappa}}\right].$$

Equation (21) can be written in dimensionless form by using the following substitutions:

$$a^* = a/\sqrt{\kappa/\delta^2\rho c}, \qquad b^* = b/\sqrt{\kappa/\delta^2\rho c}$$
$$t^* = t/\sqrt{(\delta^2\rho c/\kappa)}, \qquad H^* = h\delta/\kappa.$$

Because the assumed magnetic behavior of the material disappears as the Curie temperature is approached, temperature is normalized with respect to the Curie temperature. Then $T^* = \langle T\rangle/T_c$ where T_c is the Curie temperature and the asterisks denote dimensionless quantities. Under these substitutions the dimensionless form of (21) becomes

$$\langle T_1^*(t^*)\rangle = \frac{\langle P\rangle\delta^2}{T_c\kappa}\cdot\frac{1}{\sqrt{1-H^*}} \cdot\left[\frac{1-e^{b^{*2}t^*}\operatorname{erfc} b^*\sqrt{t^*}}{b^*} - \frac{1-e^{a^{*2}t^*}\operatorname{erfc} a^*\sqrt{t^*}}{a^*}\right]. \tag{22}$$

For $H^* = 1/4$ (22) becomes indeterminate but has a definite limiting value which is

$$\langle T_1^*(t^*)\rangle = \frac{\langle P\rangle\delta^2}{4\kappa T_c}(1-e^{t^*}\operatorname{erfc}\sqrt{t^*}), \quad \text{for } H^* = 0.25. \tag{23}$$

The steady state dimensionless temperature of the skin layer is obtained from (22) by letting $t^*\to\infty$. It is

$$\lim_{t^*\to\infty}\langle T_1^*(t^*) = \frac{\langle P\rangle\delta}{T_c h} = \frac{p}{T_c h}. \tag{24}$$

The temperature in region 2 is given by

$$\langle T_2^*(t^*, y^*)\rangle = \frac{\langle P\rangle\delta^2}{T_c\kappa}\cdot\frac{1}{\sqrt{1-4H^*}} \cdot\left\{(b^{*-1}-a^{*-1})\operatorname{erfc}\frac{1-y^*}{2\sqrt{t^*}} + a^{*-1}\,e^{a^*(1-y^*)} \cdot e^{a^{*2}t^*}\operatorname{erfc}\left(a^*\sqrt{t^*}+\frac{1-y^*}{2\sqrt{t^*}}\right) - b^{*-1} \cdot e^{b^*(1-y^*)}\,e^{b^{*2}t^*}\operatorname{erfc}\left(b^*\sqrt{t^*}+\frac{1-y^*}{2\sqrt{t^*}}\right)\right\} \tag{25}$$

where $y^* = y/\delta$. It can be shown that as $y^*\to 1$ (25) becomes identical to (22).

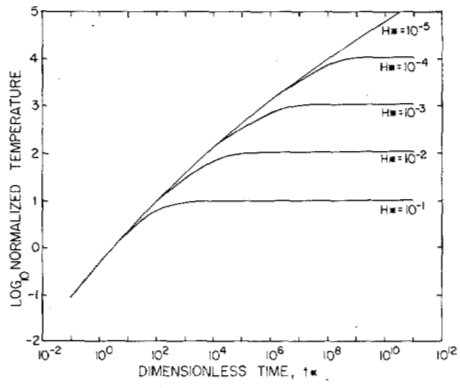

Fig. 3. Plot of variation of temperature in surface region as function of time for various values of h^*.

TABLE II
USEFUL QUANTITIES DERIVED FROM TABLE I

Material	$\rho c/\kappa$ (sec/meter^2)	h/κ (meter^{-1})*
Cobalt	5.34×10^4	0.0822-0.329
Iron	4.82×10^4	0.0754-0.302
Nickel	4.24×10^4	0.0617-0247

*h is assumed to be between 1 to 4 Btu/ft^{2}hr F or 1.357×10^{-4} to 5.43×10^{-4} cal cm^{-2} s^{-1}K.

In Fig. 3, a plot of the variation of the temperature of the surface region as a function of dimensionless time for various values of cooling coefficient, or the Nusselt number H^*, is shown. More precisely the $\log_{10} T_c\kappa\langle T_1^*\rangle/\langle P\rangle\delta^2$ is plotted against $\log_{10} t^*$. Here it is observed that the size of the Nusselt number exerts little influence on the initial heating transient. Indeed, the role of H^* is to limit the ultimate temperature that can be attained. From Table II it can be seen that the depth of penetration would have to be more than 1/3 meter for the Nusselt number to exceed 0.1, and most likely the Nusselt number is of the order of 10^{-3} to 10^{-4}.

In Fig. 4, $\langle T_2^*(t^*, y^*)\rangle/\langle T_2^*(t^*, y^* = 0)\rangle$ versus y^* for various values of t^* to show the spatial temperature distribution as a function of time is plotted. For $t^* = 0.1$ the complete thermal disturbance is confined to a region which hardly extends beyond two skin depths, that is, one skin depth for region 1 and less than one for region 2. For $t^* = 5$ the normalized interior temperature is less than $1/e$ of the temperature of region 1 at all distances from the surface greater than about 1.8. Only for the large values of t^* does the temperature disturbance reach large values of y^*.

From this very approximate linear analysis which properly accounts for ferromagnetic heating, it is concluded that a Nusselt number of zero can be assumed in the more exact calculations that follow. This is true over a very large range of values of dimensionless time t^*. The neglect of Newton surface cooling will not influence the results obtained because the heat leaving the surface is small compared to the heat being conducted to the work piece interior. In addition, it is concluded that the ferromagnetic skin depth should be adjusted to embrace the region where large temperatures are desired, because only by an extended application of power can

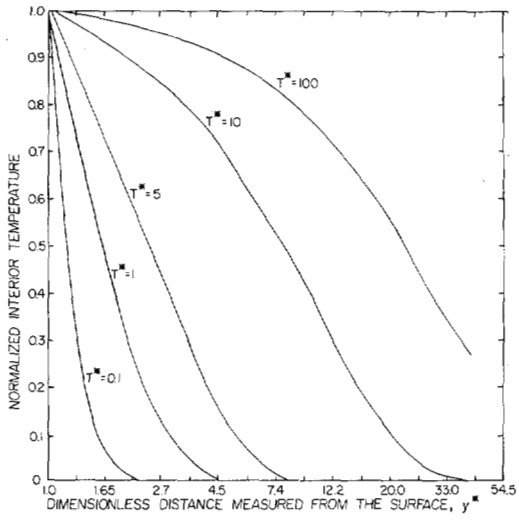

Fig. 4. A plot of normalized interior temperature as function of position at various times for $H^* = 0.0001$.

TABLE III
PROPERTIES OF IRON AS A FUNCTION OF TEMPERATURE

Temperature in °Rankine	Specific Heat	Thermal Conductivity	Electrical Conductivity 10^{-6} (MHOS/M)	Saturation Magnetization (Tesla)
400	0.0925	1.08	16.2	2.17
500	0.102	1.03	12.0	2.17
600	0.109	0.987	9.0	2.15
700	0.113	0.941	6.91	2.13
800	0.118	0.896	5.44	2.11
900	0.123	0.851	4.37	2.08
1000	0.127	0.806	3.57	2.05
1100	0.133	0.761	2.97	2.01
1200	0.141	0.716	2.50	1.98
1300	0.150	0.670	2.14	1.92
1400	0.160	0.625	1.84	1.84
1500	0.170	0.580	1.61	1.71
1600	0.183	0.535	1.41	1.57
1700	0.205	0.490	1.25	1.30
1750	0.220	0.467	1.18	1.14
1800	0.243	0.444	1.11	0.929
1850	0.320	0.422	1.05	0.500
1875	0.230	0.413	1.03	0.104
1900	0.210	0.413	0.999	0.
2000	0.182	0.415	0.926	0.
2100	0.157	0.417	0.887	0.
2200	0.130	0.419	0.869	0.
2300	0.137	0.420	0.862	0.
2400	0.143	0.422	0.860	0.
2500	0.148	0.424	0.857	0.

interior regions beyond the ferromagnetic depth of penetration be heated significantly. In applications where a high temperature, perhaps the Curie temperature, is desired in a near surface region, the electrical excitation must be adjusted so that t^* is less than unity. Then the temperature will be high in region 1 and will decay very rapidly in region 2, a distribution favorable to case hardening.

The theory just presented does not account properly for the variations in specific heat, thermal conductivity, electrical conductivity, and saturation magnetization which exist over the temperature range from room temperature to the Curie temperature. Inspection of Table III indicates that electrical con-

TABLE IV
THE SOLUTION TO THE IDEALLY INSULATED SKIN REGION

T in °R	$10^{-8} \times I(T)$ in amperes per meter
528	0
566	0.126
638	0.378
776	0.882
1026	1.89
1241	2.90
1336	3.402
1359	3.528
1402	3.78
1444	4.032
1520	4.536
1588	5.04
1649	5.544
1663	5.67
1676	5.796
1700	6.048
1743	6.552
1809	7.56
1831	8.064
1846	8.568
1849	8.694
1855	8.946
1860	9.198
1863	9.29
1868	9.61
1875	10.24
1877	10.55
1879	11.18
1880	12.60

ductivity and especially saturation magnetization undergo the most change. Hence the thickness of region 1 changes greatly as the temperature rises to the Curie point. An estimate of magnetic intensity or frequency to obtain any temperature and skin depth in a certain time would not be accurate or even correctly based on this simplified theory. In case hardening it is desirable to confine the heating to region 1. That is possible by maintaining values of dimensionless time near unity. If that is done (18) becomes

$$H_m f\tau = 3/8\rho \int_{T_R}^{T} \frac{C(x)}{B_s(x)}\, dx = I(T) \tag{26}$$

where τ is the time required to raise region 1 from T_R, room temperature to an elevated temperature T. Here it is assumed that no heat flows out of region 1. The value of the integral $I(T)$ is given in Table IV. We note that $I(T)$ depends only on temperature and the temperature variations of heat capacity and saturation induction. Hence, for any desired temperature rise in region 1, the frequency, the magnetic intensity, and the required time can be adjusted in anyway that satisfies (26).

DETERMINATION OF EXCITATION REQUIREMENTS

In case hardening applications it may be desirable to heat a near surface region of a certain thickness up to the Curie temperature in a given amount of time. Although the time may not be specified, the shorter the heating time, the higher the temperature gradients and the more confined the heating. For example, it is assumed that a near surface area of a workpiece is to be heated up to 1880°R in 0.36 seconds. From Table III, $I(1880) = 12.6 \times 10^8 = H_m f\tau$ where τ is the heating time. Then, if the available source of power has a frequency of 350 Khz, $H_m = 12.6 \times 10^8/0.36 \times 3.5 \times 10^5 \simeq 10{,}000$ amperes per meter. Making use of the standard formula for electromagnetic skin depth $\delta = (\pi f \sigma \mu_o)^{-0.5}$, and using the value of conductivity given in Table IV for a temperature of 1880°R, $\delta = 0.842$ mm. Although the expressions given by (22) and (25) are not accurate because of the assumption of κ, c, σ and B_s not being functions of temperature, it is still instructive to inspect the values of dimensionless variables obtained. For example, at $T = 1880$°R and for $\tau = 0.36$ s, $t^* = 0.048$. This seems to indicate that only region 1 will be heated to the vicinity of the Curie temperature. Equations (25) and (26) do not yield any quantitative information about the transient temperature distribution in region 2. Equation (25) completely ignores the fact that specific heat, thermal conductivity, and saturation magnetization are strong functions of temperature. Equation (26) assumes region 2 is an insulator, and properly accounts for the thermal variations of the physical properties of iron. Qualitatively, (25) indicates that the temperature in region 1 falls considerably in a distance of a few electrical skin depths. For excitation of $H_m = 10\,000$ amps/meter and $f = 350$ kilohertz the electrical skin depth ranges between about 0.019 to 0.84 mm depending upon temperature. The normalization of (25) could have been accomplished another way by using the quantity $d = (\kappa\tau/\rho c)^{1/2}$ to make y dimensionless. If $\tau = 0.36$ s then $0.2 < d \leqslant 0.4$ mm. Hence, from (25) and Fig. 4 it is estimated that the material several skin depths or in this case several millimeters beyond region 1 will attain a temperature much lower than region 1 during the heating time τ. To be more specific, a numerical solution to (19) and (5) must be executed.

THE NUMERICAL SOLUTION

It would be desirable to numerically solve (5) and (6) simultaneously, accounting for the temperature variations in κ, c, σ and μ_{inc}. However, it is difficult to get data on μ_{inc}, the incremental permeability as a function of temperature, and μ_{inc} depends upon past heat treatments. Also, the work of Merewether [6] indicates certain numerical difficulties which become worse as the frequency is raised. Instead, in region 2 the nonlinear heat flow equation (5) is solved simultaneously with the average nonlinear heat flow equation (19) valid in region 1. Here the average power density is obtained from the limiting nonlinear analysis previously explained. In addition to the relationships already stated, the saturation induction is given by

$$B_s = \mu_o H_m + M_s \tag{27}$$

and M_s; the saturation magnetization is plotted as a function of temperature in Fig. 5. Equation (7) is used at all temperatures, and with the assumption of (27) is valid at both room temperature, any temperature where $B_s/H_m \gg \mu_o$, and at the Curie temperature and above. The saturation magnetization drops very rapidly within a few degrees of the Curie tempera-

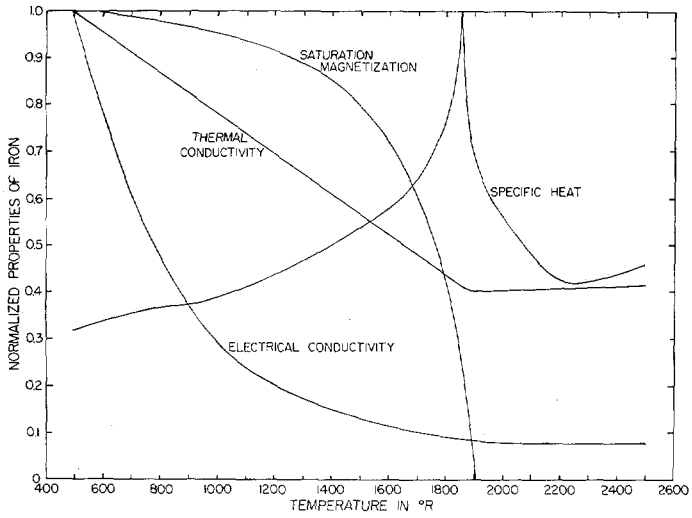

Fig. 5. The thermophysical properties of iron as function of temperature.

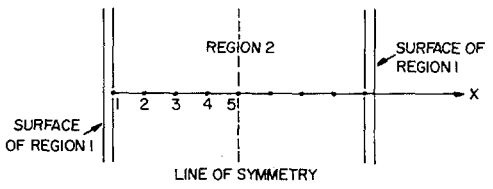

Fig. 6. Numerical solution grid.

ture as shown by Fig. 5. In that small temperature range this approximation of (7) may be somewhat inaccurate. This constitutes a transition between the limiting nonlinear and the standard linear theory of eddy current phenomena in solid iron. Under the approximation of (27) the transition is a smooth one. Only a small fraction of the total heating time is spent in the transition regime. Equation (11) is used for the average power per unit volume until the transition is completed; then (15) is used. Region 2 is characterized by $2N - 1$ points at which the temperature is sought as shown in Fig. 6. Due to symmetry only half of the geometry is considered. In Fig. 6 $N = 5$. The finite difference-differential equation for point 1 is given by (19) as

$$\frac{dT_1}{dt} = [\langle\kappa\rangle (T_2 - T_1)/y_o \delta(T_1) + \langle P(T_1)\rangle] / \rho c(T_1) \qquad (28)$$

where $\langle\kappa\rangle$ is a mean value of thermal conductivity given by $\langle\kappa\rangle = [\kappa(T_2) + \kappa(T_1)]/2$. The finite difference-differential equation for the remaining points of interest derives from (5) and is given by

$$\frac{dT_i}{dt} = \{\kappa(T_i)\, T_{i+1} - [\kappa(T_i) + \kappa(T_{i-1})]\, T_i + \kappa(T_{i-1})\, T_{i-1}\} / y_o^2 \rho c(T_i), \qquad (29)$$

valid for $i \leqslant 2 \leqslant N - 1$. This equation was obtained by using a forward difference for the first differentiation and a backward difference for the second. At the middle of region 2 there is symmetry and no heat flows, or $\partial T/\partial y = 0$ there. To accomplish this we set $T_{N+1} = T_{N-1}$ to yield the equation

$$\frac{dT_N}{dt} = \{2\kappa(T_{N-1})\, T_{N-1} - [\kappa(T_N) + \kappa(T_{N-1})]\, T_N\} / y_o^2 \rho c(T_N) \qquad (30)$$

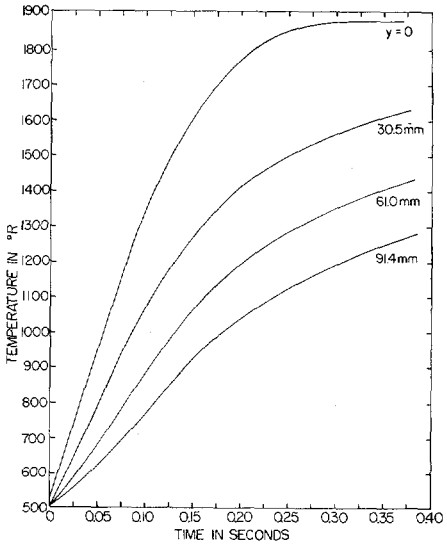

Fig. 7. Plot of temperature versus time at various values of position. Here $H_m = 10^4$ amp/meter, $f = 350$ kilohertz, and $y_o = 1.2$ inches.

valid for $i = N$ only. The right sides of these functions are given elsewhere in the notation of APL [8]. The remaining boundary condition is obtained by specifying the film coefficient h. As long as h is kept within physically obtainable limits it has little influence on initial heating transients and can be assumed to be zero. The averaging process from whence (19) and (28) are derived automatically includes the boundary condition on the air-iron interface of region 1. The initial condition on temperature depends on the situation, but is taken in this work to be $T_i = 528°$R for $t = 0$. APL functions for the thermophysical properties of iron corresponding to Fig. 5 and Table III are included [8]. The differential-difference technique of Petrov [7] is used to solve (28), (29), and (30). Essentially, the method solves N simultaneous nonlinear first order differential equations, one at each point in space, by a numerical integration such as the Runge-Kutta method. Petrov shows this technique to be more efficient than most other methods, and establishes a limit on the size of time step which may be used to obtain an accurate solution. For an excitation of $H_m = 10\,000$ amps/m and $f = 350$ kilohertz, a numerical soltuion containing 17 points for a half-sheet was executed. An increment of $y_o = 1.2$ inches was chosen to insure quick computation and good convergence. The results are shown in Figs. 7 and 8. From Fig. 7 we note that the Curie temperature is reached by region 1 in 0.36 seconds, as would be predicted by (26) and Table IV. Only the first four points in distance are represented in Fig. 7. In Fig. 8 plots of temperature distribution at $t = 0$, 0.054, 0.108, 0.153, and 0.364 seconds after the thermal transient is initiated are shown. When the temperature of region 1 is 1880°R, the "thermal skin depth" of region 2 corresponds to the place where the temperature is 1025°R. This occurs at about 0.16 meters from the interface between regions 1 and 2. At the interface the temperature gradient is estimated to be about 10°R per millimeter when region 1 has reached the Curie tem-

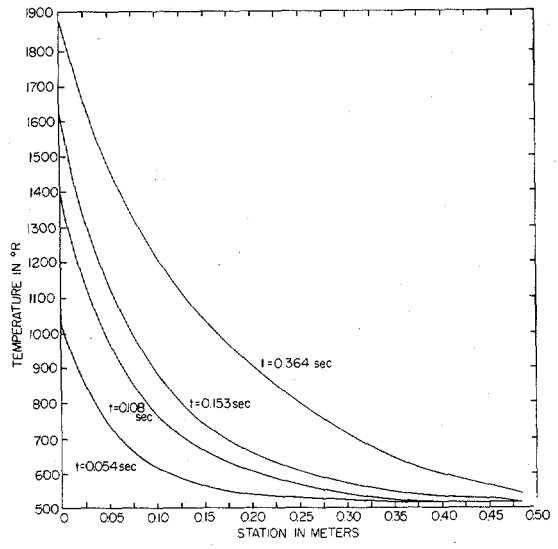

Fig. 8. Plot of temperature versus position at various values of time. Here $H_m = 10^4$ amp/meter, $f = 3500$ kilohertz, and $y_o = 0.12$ inch.

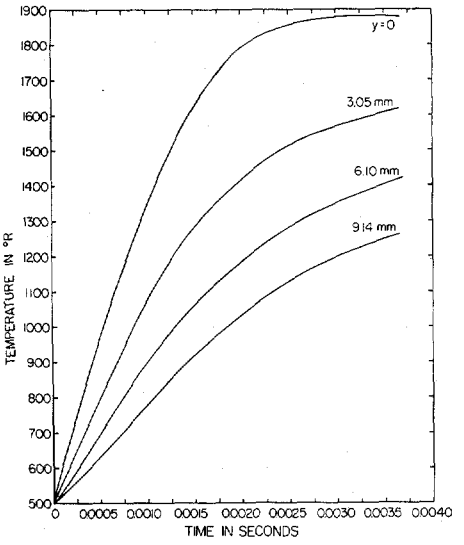

Fig. 10. Plot of temperature versus time at various values of position. Here $H_m = 10^5$ amp/meter, $f = 3500$ kilohertz, and $y_o = 0.12$ inch.

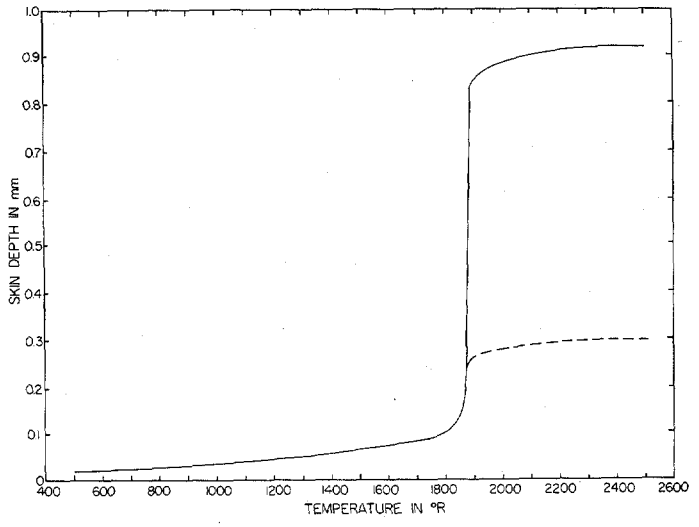

Fig. 9. The thickness of region 1 as a function of temperature for two different excitations. (– – – for $H_m = 10^5$ amp/meter and $f = 3500$ kilohertz, ——— for $H_m = 10^4$ amp/meter and $f = 350$ kilohertz).

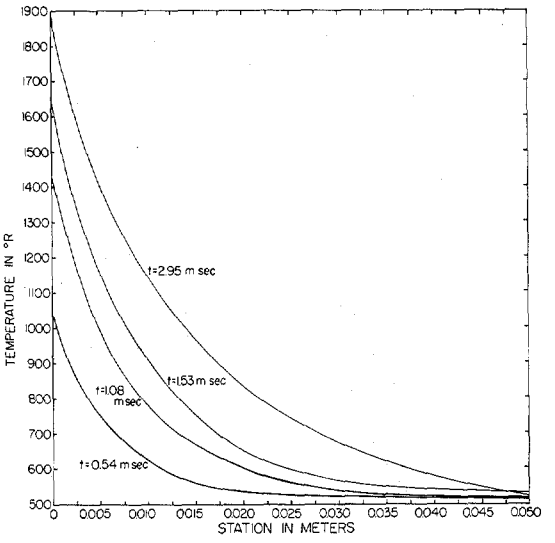

Fig. 11. Plot of temperature versus position at various values of time. Here $H_m = 10^5$ amp/meter, $f = 3500$ kilohertz, and $y_o = 0.12$ inch.

perature and region 1 is 0.84 millimeters thick. In Fig. 9 the thicknesses of region 1 under different conditions is shown. Below 1850°R both curves are the same because the ratio of H_m/f is the same in both cases. Thus, when region 1 behaves as a ferromagnetic material the thickness of region 1 is about 0.0187 mm for both excitations. However, raising H_m from 10^4 to 10^5 amps/meter and raising the frequency from 350 to 3500 kilohertz requires a hundredfold increase in power per unit volume dissipated in the ferromagnetic region. The numerical solution for $H_m = 10^5$ amps/meter and $f = 3.5$ megahertz was executed with $y_o = 0.1$ and 0.01 meters. The latter results are presented in Figs. 10 and 11. The figures are similar except the abscissa scale of Fig. 10 is 0.01 that of Fig. 7 and the abscissa scale of Fig. 11 is one tenth that of Fig. 8. The former observation is in agreement with (26) and Table IV. The latter observation indicates that the "thermal skin depth" dropped but one order of magnitude when the Curie heating time dropped two orders of magnitude. The thickness of region 1 at 1880°R is 0.266 mm and the temperature gradient at the interface between regions 1 and 2 is about 320°R/mm. During the time when region 1 is heating to the Curie temperature, the heat being conducted into region 2 is small compared to the heat being stored in region 1. Then by (19) the time rate of increase of temperature is proportional to the power per volume dissipated in region 1. Since most of the heating occurs when the iron is ferromagnetic, the time rate of temperature increase in region 1 is proportional to the product of the magnetic intensity and frequency. The temperature at point 1 is the temperature of region 2 at its interface with region 1. Just after region 1 reaches the Curie temperature the power dissipated becomes smaller by almost two orders of magnitude than it was when region 1 was ferromagnetic. This is illustrated in Fig. 12. Then by (19) the term P becomes

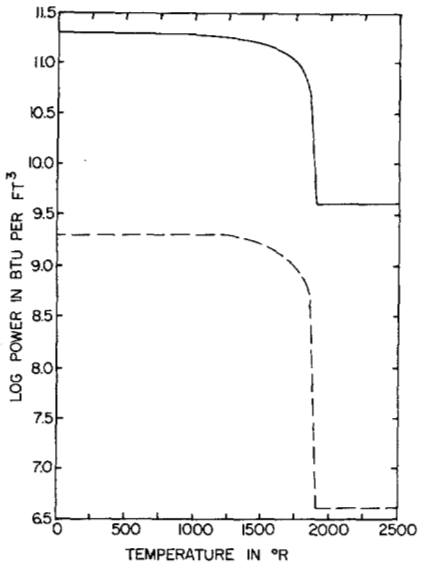

Fig. 12. Plot of $\log_{10}$ of power in region 1 versus temperature (– – – for $H_m = 10^4$ amp/meter and 350 kilohertz, and ——— for $H_m = 10^5$ amp/meter and 3500 kilohertz).

small compared to

$$\rho c \partial \langle T \rangle / \partial t \quad \text{and} \quad (\partial T/\partial y)|_{y=\delta} \simeq \rho c \delta \frac{\partial \langle T \rangle}{\partial t} \simeq \rho c \delta H_M f.$$

Here δ is the ordinary electric skin depth proportional to $f^{-1/2}$. Therefore, a good estimate of the temperature gradient at the left boundary of region 2 is given by

$$\left.\frac{\partial T}{\partial y}\right|_{y=\delta} = \beta H_m \sqrt{f} \tag{31}$$

where β is a constant of proportionality. From Fig. 8 an estimate of β is found to be 1.69×10^{-6} or meter $\sec^{1/2}$/amp mm. If (31) is applied to the case where $H_m = 100\,000$ amps/meter and $f = 3.5 \times 10^6$ hertz, it is found that the temperature gradient is 316°R/mm, which agrees well with the numerical solution of Fig. 11.

Conclusions

The heat transfer between the work piece and the surrounding air is negligible compared to the heat conducted toward the interior for practical Nusselt numbers. It has been shown that to heat a near surface region to any given temperature, the product of the applied magnetic field intensity, frequency of excitation, and desired heating time must equal a certain value. This value, given for iron in Table IV, is related to the temperature and density of the material and the way the heat capacity and saturation induction of the material vary with temperature. The application of this criterion yields a heated near surface region whose depth is the electromagnetic depth of penetration. Beyond the near surface region the temperature diminishes rapidly. The gradient of the temperature just beyond the near surface region is proportional to the product of the applied magnetic field intensity and the square root of the excitation frequency. In industrial practice the frequency of excitation may not be easy to vary. If that is the case, the thickness of the near surface region to be heated to near the Curie point is determined by the fixed frequency and the electrical conductivity of the material at the elevated temperature, and the designer has no control over this quantity. By (31) the temperature gradient just outside of the heated region can be adjusted by the proper choice of H_m the applied magnetic field intensity. Then by (26) the heating time is determined. Alternatively, the heating time can be chosen and H_m can be obtained from (26). The resulting temperature gradient outside the heated region is predicted from (31). When the frequency is fixed there is not much flexibility in the design of near surface heating apparatus. If the applied magnetic intensity is chosen for convenience or practical reasons, then the resulting heating time and thermal gradient must be tolerated. If it is possible to choose the applied magnetic field to produce the desired thermal gradient then the heating time dictated by (26) must be accepted.

In summary, it has been shown how heating time, applied magnetic field intensity, desired temperature, heating thickness, and temperature gradient are related, taking into account all of the complicated thermophysical properties and properly considering the nonlinear magnetic properties of ferromagnetic materials. For any given ferromagnetic material, equations similar to (26) and (31) can be derived as they have been for iron. From these equations it is possible to understand better the induction heating processes required in case hardening.

Appendix

Here (16) and (19) are solved to obtain the thermal transient in the magnetic skin layer given by (21). By Laplace transformation with respect to time, (16) and (19) become

$$(\rho c \delta s + h) \langle t_1(s) \rangle = \frac{P\delta}{s} + \left.\frac{\kappa dt_2(s,y)}{dy}\right|_{y=\delta} \tag{32}$$

(where the last term is a consequence of Fourier's law of heat conduction at $y = \delta$ and the convention that $L[T(t, y)] = t(s, y)$ is used) and

$$\frac{\kappa d^2 t_2(s,y)}{dy^2} - s\rho c t_2(s,y) = 0. \tag{33}$$

The solution to (33) is

$$t_2(s,y) = A(s) \exp\left(-y\sqrt{s\rho c/\kappa}\right) \tag{34}$$

where $A(s)$ is a constant of integration. From (34)

$$[dt_2(s,y)/dy]|_{y=\delta} = -\, t_2(s,\delta)\sqrt{s\rho c/\kappa}.$$

However, at $y = \delta$, $t_2(s, \delta) = \langle t_1(s, \delta) \rangle$ and thus

$$A(s) = \langle t_1(s) \rangle \exp\left(\delta\sqrt{s\rho c/\kappa}\right). \tag{35}$$

Then (34) becomes

$$t_2(s,y) = \langle t_1(s) \rangle \exp\left[(\delta - y)\sqrt{s\rho c/\kappa}\right] \qquad \text{for } y \geqslant \delta \text{ only} \tag{36}$$

where $\langle t_1(s) \rangle$ must be found before (36) can be inverted. The right most member of (32), found just below (34), is substi-

tuted into (32) to yield

$$(\delta\rho cs + h + \sqrt{s\rho c/\kappa})\,\langle t_1(s)\rangle = \frac{P\delta}{s}. \tag{37}$$

By means of certain algebraic manipulations (37) can be cast in the form

$$\langle t_1(s)\rangle = \frac{P}{s\rho c\sqrt{(\kappa/\delta^2\rho c) - (4h/\rho c\delta)}}\left(\frac{1}{\sqrt{s}+b} - \frac{1}{\sqrt{s}+a}\right) \tag{38}$$

where a and b are the same as those given in (21). Equation (38) is comprised of simple standard Laplace transforms, easily inverted to yield the result previously stated in (21). The $\langle t_1(s)\rangle$ of (38) can be substituted into (36) to yield $t_2(s, y)$. The resulting $t_2(s, y)$ can also be inverted and leads to a somewhat more complicated result than (21). The result is given by (25).

References

[1] C. A. Tudbury, *Basics of Induction Heating*, Rider 1960.
[2] C. A. Tudbury, "Electromagnetics of Induction Heating," *IEEE Trans. Mag*-10, 694-697, September 1974.
[3] F. J. Young, "Pulse Shielding by Nonferrous and Ferromagnetic Materials," in *Proceedings IEEE*, 61, 404-413, April 1973.
[4] H. M. McConnell, "Eddy-Current Phenomena in Ferromagnetic Materials," *AIEE Trans.*, 73, 266-235, July 1954.
[5] P. D. Agarwal, "Eddy-Current Losses in Solid and Laminated Iron," *AIEE Trans.*, 78, 169-179, May 1959.
[6] D. E. Merewether, "Electromagnetic Pulse Transmission Through a Thin Sheet of Saturable Ferromagnetic Material of Infinite Surface Area," *IEEE Trans. Electromagn. Compat.*, EMC-11, 139-143, November 1969.
[7] A. A. Petrov "A Differential-Difference Technique for the Hybrid Computer Solution of Parabolic Partial Differential Equations," Annales de l' Association internationale pour le Calcul analogique, #2, pp. 104-109, April 1975.
[8] F. J. Young, "Algorithms used in Induction Heating for Case Hardening," NAPS document #03155 available from ASIS/NAPS, c/o Microfiche Publications, P. O. Box 3513, Grand Central Station, New York, N.Y. 10017.

Letters

A True Swap Gate for Magnetic Bubble Memory Chips

P. I. BONYHARD

Abstract—**The design of a true swap gate suitable for incorporation into magnetic bubble memory chips with 16-μm to 18-μm circuit periods is reported. The swap operation is true in that the outcoming bubble takes the position vacated by the ingoing bubble, as well as vice versa. Swap gates of this design have been operated successfully at temperatures from 0°C to 70°C, and frequencies up to 100 kHz.**

The design of a swap gate, as well as other functions, suitable for incorporation into magnetic bubble memory chips with circuit periods of 16 μm to 18 μmm has been reported [1]. The swap gate reported did not place the bubble taken out of the storage loop into the position vacated by the ingoing bubble. Also, the design of the storage loop turn at the swap gate was not fully satisfactory in that this turn propagated only over a bias field margin range considerably less than the margin range for a propagate along a straight path.

A superior design is shown in Fig. 1. The storage loops are on 36-μm centers and the nominal minimum feature size is 2 μm, as in the earlier design. An improved version [2] of the asymmetric half disk propagate element [1] is used. The swap operation is true in that not only does the ingoing bubble go into the position vacated by the outcoming bubble, but also vice versa. The 180° storage loop turn incorporated in this design has been found in no way to limit the bias field margin range of the loop. The propagate margin range of the write major line, however, can be the margin limiting feature on the chip, depending on circuit processing, especially at rotating drive fields of about 30 Oe and less.

Swap gates of this design have been operated successfully on a large number of chips, in wafers, and in packages at temperatures from 0°C to 70°C, rotating drive field frequencies of 50 kHz to 100 kHz, and amplitudes of 35 Oe to 55 Oe. Swap current amplitudes of 30 mA ± 10% have been used successfully in most tests, but successful operation

Manuscript received May 2, 1977.
The author is with Bell Laboratories, Murray Hill, NJ 07974.

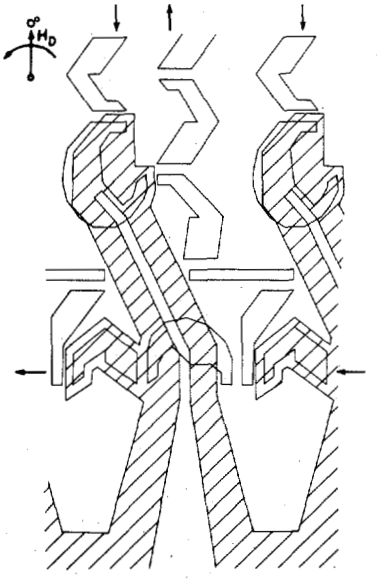

Fig. 1. True swap gate.

at 30 mA ± 33% has also been demonstrated in some cases. Phase margin ranges, like those of most transfer type bubble functions, are very wide and have not been fully investigated. "On" phases from 270° to 330° and "off" phases from 640° to 700° are known to work satisfactorily.

Acknowledgment: The author wishes to express his thanks to his colleagues who produced and helped to characterize the circuits.

References

[1] P. I. Bonyhard and J. L. Smith, "68 kbit capacity, 16 μm-period magnetic bubble memory chip design with 2 μm minimum features," *IEEE Trans. Mag.*, MAG-12, pp. 614-617, Nov. 1976.
[2] A. H. Bobeck, "The development of bubble memory devices," to be published in the *Proceedings of Electro* 77.